Numerical simulations of conjugate convection combined with surface thermal radiation using an Immersed-Boundary Method

F. Favre[1], G. Colomer[1,2], O. Lehmkuhl[1], A. Oliva[1]

[1]Heat and Mass Transfer Technological Centre (CTTC), Universitat Politcnica de Catalunya (UPC), ESEIAAT, Colom Street 11, E08222, Terrassa (Barcelona), Spain.
[2]Termo Fluids S.L., Avinguda Jaquard, 97 1-E, E08222, Terrassa (Barcelona), Spain.

E-mail: federico@cttc.upc.edu

Abstract. Dynamic and thermal interaction problems involving fluids and solids were studied through a finite volume-based Navier-Stokes solver, combined with immersed-boundary techniques and the net radiation method. Source terms were included in the momentum and energy equations to enforce the non-slip condition and the conjugate boundary condition including the radiative heat exchange. Code validation was performed through the simulation of two cases from the literature: conjugate natural convection in a square cavity with a conducting side wall; and a cubical cavity with conducting walls and a heat source. The accuracy of the methodology and the validation of the inclusion of moving bodies into the simulation was performed via a theoretical case

1. Introduction

The problem of conjugate heat transfer combined with surface radiative exchange has many industrial applications such as the design of energy efficient buildings, heat-loss analysis of furnaces, cooling of electronic equipment, etc. Therefore, the development of efficient and tested computational tools to study these phenomena is needed. CFD-based codes can produce reliable fields of flow, temperature and heat flux, useful for identifying potential design problems.

In the present work, an immersed-boundary method (IBM) implemented in our in-house code TermoFluids [1] presented in an earlier work [2] was improved to simulate the mentioned phenomena. This allows to simulate thermal flow problems including moving and/or deforming bodies in static grids. These approaches impose the boundary condition, reconstructing the solution in the vicinity of the bodies. In this way, it is possible to force the non-slip condition for the momentum equation and the conjugate condition for the energy equation.

2. Numerical method

2.1. Navier-Stokes solver

The spatial discretized Navier-Stokes equations can be written as,

$$\mathcal{M}\boldsymbol{u}_c = \mathbf{0} \tag{1}$$

$$\Omega\frac{\partial \boldsymbol{u}_c}{\partial t} + \mathsf{C}\left(\boldsymbol{u}_c\right)\boldsymbol{u} + \nu\mathsf{D}\boldsymbol{u}_c + \rho^{-1}\Omega\mathsf{G}\boldsymbol{p} + \boldsymbol{f} = \mathbf{0} \tag{2}$$

$$\Omega\frac{\partial T}{\partial t} + \mathsf{C}\left(\boldsymbol{u}_c\right)T + \frac{\lambda}{c_p\rho}\mathsf{D}T + s = \mathbf{0} \tag{3}$$

where $\mathcal{M}$, $\mathsf{C}(\boldsymbol{u}_c)$, D and G are the divergence, convective, diffusive and gradient operators respectively, Ω is a diagonal matrix with the sizes of control volumes, ρ is the fluid density, ν is the viscosity, $\boldsymbol{p}$ represents the pressure, $\boldsymbol{u}_c$ is the velocity, T is the temperature, λ is the thermal conductivity, c_p is the specific heat and $\boldsymbol{f}$ and s are the source terms included due to the immersed boundaries.

The governing equations have been discretised on a collocated unstructured grid arrangement by means of second-order, spectro-consistent schemes. The conservative nature of these schemes ensures the preservation of the symmetry properties of the continuous differential operators and ensures both the stability and conservation of the kinetic-energy on any grid.

A fractional-step method was employed to perform the time integration of the equations. The convective and diffusive terms were explicitly treated with a self-adaptive strategy using the κ1L2 method [3].

2.2. Boundary Reconstruction

The immersed bodies were represented by triangular surface meshes in stereo-lithography format (STL) allowing the handling of intricate geometries [5]. A signed minimum distance field was calculated in the pre-process from the control volume centroids to the bodies surface to classify nodes in interior, exterior, interior-forcing and exterior-forcing points as shown in figure 1.

The procedures utilized to reconstruct the solution at the interface of the bodies are described in the following sub-sections.

2.2.1. Momentum The time integration of the momentum equation was performed as follows:

$$\frac{\overrightarrow{u_P} - \overrightarrow{u^n}}{\Delta t} = RHS^n + \overrightarrow{f} \tag{4}$$

where $\overrightarrow{u_P}$ is the predictor velocity, $\overrightarrow{u^n}$ is the velocity at time step n and RHS^n includes the convective and diffusive terms. $\overrightarrow{u_P}$ was first obtained by imposing $\overrightarrow{f} = 0$ in this equation, and the value of $\overrightarrow{f}$ was then calculated to impose the desired value $\overrightarrow{V}$ in the corresponding nodes:

$$\overrightarrow{f} = \frac{\overrightarrow{V} - \overrightarrow{u^n}}{\Delta t} - RHS^n \tag{5}$$

$$\overrightarrow{V} = a_W\overrightarrow{u}_W + a_{nb1}\overrightarrow{u}_P^{nb1} + a_{nb2}\overrightarrow{u}_P^{nb2} + a_{nb3}\overrightarrow{u}_P^{nb3} \tag{6}$$

Given the movement of the immersed body, the value of $\overrightarrow{V}$ for the interior and interior-forcing points was directly calculated from their coordinates. An approximation is needed in the case of exterior-forcing points, since by definition these nodes are located outside the object. A second-order interpolation is thus employed, which maintains the global accuracy of the scheme (Fadlun *et al.* [4]). Four velocities were used in this process (see equation 6): one refers to the closest point of the object and the remaining three are velocities of exterior nodes which are

neighbours of the forcing point. Coefficients were calculated making exclusive use of geometrical information.

The obtained value of $\overrightarrow{f}$ was then introduced in equation 4 to calculate $\overrightarrow{u_P}$. With this new field of $\overrightarrow{u_P}$, Poisson equation was solved and the velocity field $\overrightarrow{u}^{n+1}$ updated (see equations 7 and 8).

$$\mathsf{D}\boldsymbol{p}^{n+1} = \frac{1}{\Delta t}\mathcal{M}\overrightarrow{u_P} \tag{7}$$

$$\overrightarrow{u}^{n+1} = \overrightarrow{u_P} - \Delta t \mathsf{G}\boldsymbol{p}^{n+1} \tag{8}$$

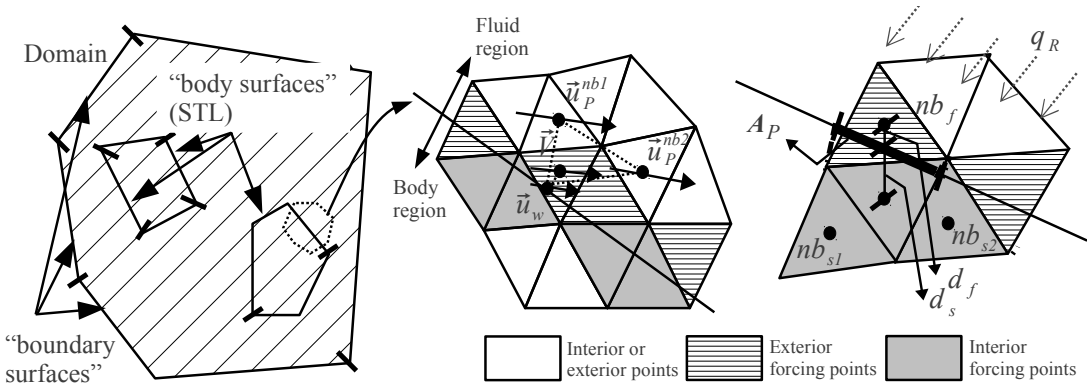

Figure 1. Representative domain and example of Control Volumes intersected by an object.

2.2.2. Energy In the energy equation, the term s forces the boundary condition in the bodies interfaces, therefore has a zero value in the exterior and interior points. For a Dirichlet or a Neumann condition, a desired value of temperature (T^*) for each forcing point was calculated by interpolation, using the same neighbours and coefficients as for the estimation of V. After T^* was obtained, s could be calculated as shown in equation 10.

$$\frac{T^{n+1} - T^n}{\Delta t} = RHS^n + s \tag{9}$$

$$s = \frac{(T^* - T^n)}{\Delta t} - RHS^n \tag{10}$$

For the conjugate problem, for which no temperature value can be imposed, s was calculated so that the heat fluxes were corrected taking into account the interface. Equation 11 was employed to that end: q_I is the heat exchange between the forcing point and the other region; and q_{Nb} is the heat exchange between the forcing point and the neighbours of the same region. Equations 12 and 13 show these calculations for an interior forcing point. A_f is the area of the face between centroids, m_f is the incoming mass through that face, $\vec{d}$ is the distance between centroids and $\vec{n}$ is the normal to the face pointing to the exterior of the solid.

$$s = q_I + q_{Nb} + S - RHS^n \tag{11}$$

$$q_I = \frac{1}{Vol\rho}\sum_{nbf_i}\left[\frac{A_f(d_s + d_f)}{(\vec{n}\cdot\vec{d})c_P}\left(\frac{d_s}{\lambda_S} + \frac{d_f}{\lambda_F}\right)^{-1}(T^n_{nbfi} - T^n) + m_f(T^n_{nbfi} - T^n)\right] \tag{12}$$

$$q_{Nb} = \frac{1}{Vol\rho}\sum_{nb_{si}}\left[\frac{A_f\lambda_S}{(\vec{n}\cdot\vec{d})c_P}(T^n_{nbsi} - T^n) + m_f(T^n_{nbsi} - T^n)\right] \tag{13}$$

Moreover, in the interior forcing points a source term S was included for external heat sources as radiation. S was calculated by equation 14, where A_p is the projected area of the cell into the body's interfaces, and q_R is the radiative heat per unit area —its calculation is explained in the following section.

$$S = q_R \times A_p/(c_P \rho Vol) \tag{14}$$

2.3. Radiative transfer equation

The net radiation problem was solved [6] to calculate the term q_R from equation 14. Two kinds of surfaces are involved in the problem: those from boundaries of the domain, referred to as "boundary surfaces" in Figure 1, and (ii) those from the immersed bodies, "body surfaces". For both cases, surfaces were defined as a group of faces selected in the pre-process. The number of surfaces depend on the nature of the problem, therefore, the radiative problem could range from enormously costly to nearly neglectable.

Once the surfaces were defined, the areas were computed and stored. The view factors were calculated using ray-tracing [6, 7], an operation that must be repeated when at least one body moves. The mean temperatures of the surfaces were calculated in each time step for both "boundary surfaces" and "body surfaces". For the latter, the calculation was done via interpolation, using the information of the interior forcing points. The radiation system was solved by the GMRES [8] iterative solver, based on Krylov subspace projection methods. Finally, the heat fluxes were set to the faces. For the "body surfaces" S is computed using equation 14, while for the "boundary surfaces" it is directly calculated using the face areas.

3. Results

3.1. Case 1. Square cavity with a conducting side wall

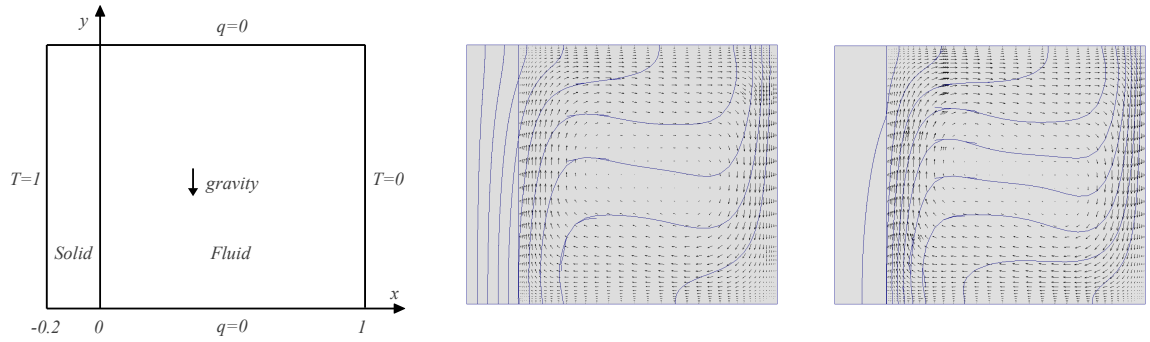

(a) (b) (c)

Figure 2. (a) Scheme of the conjugate natural convection problem. (b) Isothermal lines and velocity vectors for K=1 and for (c) K=5.

A benchmark case, widely used in conjugate heat transfer problems, was employed to perform the first validation of the code. It is a natural convection problem which consists of a square cavity with a conducting side wall for which the results from [9] are available. The cavity is heated at the left side (solid wall) keeping a constant temperature, and cooled at the right side. All the remaining boundaries are considered adiabatic. For the fluid domain, all boundaries have the no-slip velocity boundary condition.

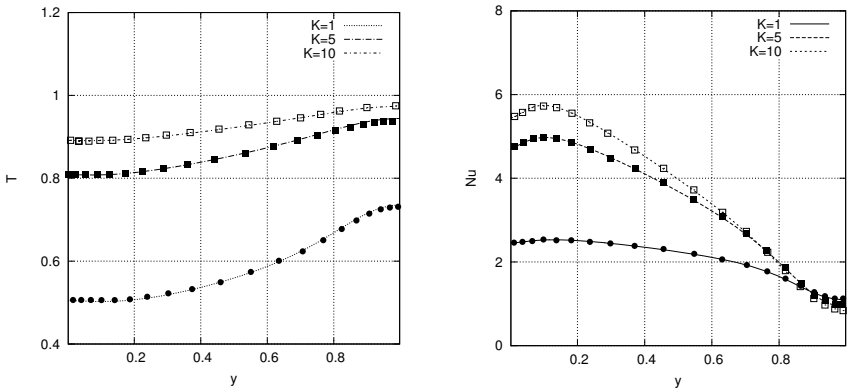

Figure 3. (a) Temperature and (b) Nusselt number distributions at the interface line $x = 0$. Lines: reference results. Points: present results.

The computational mesh employed consisted of 14×40 CV in the solid domain, with exponential densification close to the interface and 40×40 CV in the fluid domain, with hyperbolic densification close to the walls. Air with $\mathrm{Pr} = 0.71$ was utilized as the working fluid. The test case is of Rayleigh number 71000 and was solved for three thermal conductivity ratios $K = \lambda_{solid}/\lambda_{fluid}$: 1, 5 and 10.

Local comparisons of temperature and Nusselt number distribution along the interface center line are shown in Figure 3. The good agreement of these local distributions with the benchmark data for the three ratios of thermal conductivity confirms the adequate performance of the methodology.

3.2. Case 2. Cubical heated cavity with conducting walls

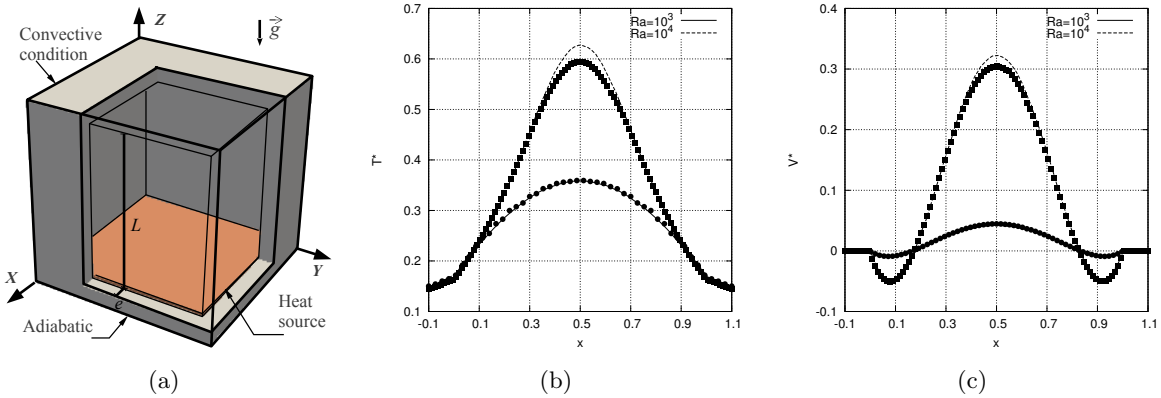

Figure 4. (a) Scheme of a cubical heated cavity with conducting walls. (b) Temperature and (c) vertical velocity distributions at the central line $Y = Z = 0.5$. Lines: reference results. Dots: present results.

A surface thermal radiation and conjugate heat transfer case presented by Martyushev et. al. [10] was employed as a second validation of this work. It consists of a cubical enclosure with

heat-conducting solid walls of finite thickness. At the bottom, in contact with the fluid, a heat source is located which maintains the superficial temperature at T_{max}. The exterior walls lose heat by convection with an external fluid at T_{min}. The inferior surface, however, is defined as adiabatic. The configuration is schematically shown in Figure 4(a).

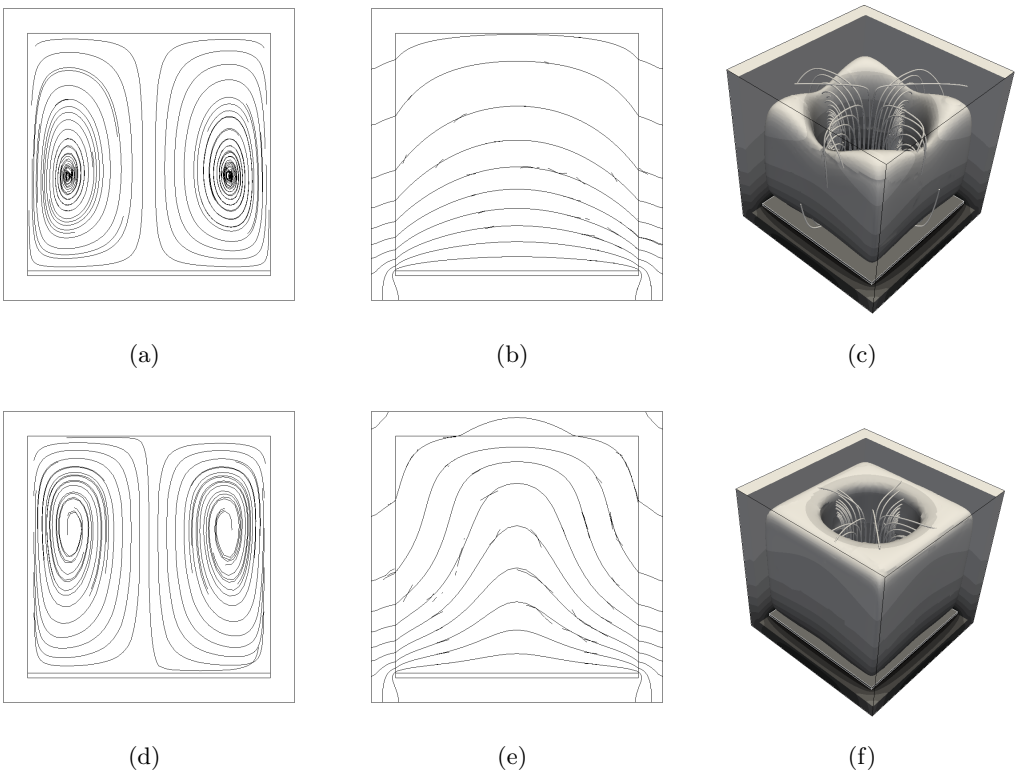

Figure 5. Results for $Ra = 10^3$: (a) streamlines and (b) isothermal lines at $X = 0.5$, (c) 3D view of streamlines and contour plots of V. Results for $Ra = 10^4$: (d) streamlines and (e) isothermal lines at $X = 0.5$, (f) 3D view of streamlines and contour plots of V.

To completely define the case, the following non-dimensional numbers were specified: Planck $Pl = \lambda_{fluid}(T_{max} - T_{min})/(\sigma T_{max}^4 L)$, Biot $Bi = hL/\lambda_{solid}$, Raiyleigh $Ra = g\beta(T_{max} - T_{min})L^3/\nu\alpha_{fluid}$ and the ratio $K = \lambda_{solid}/\lambda_{fluid}$, where λ is the thermal conductivity, σ is the Steffan-Boltzman constant, h is the external coefficient of convection, β is the coefficient of volumetric thermal expansion, ν is the kinematic viscosity and α is the thermal diffusivity of the fluid.

Two cases were simulated: for the first case, values of $Ra = 10^3$ and $Pl = 0.4566$ were used, and for the second case $Ra = 10^4$ and $Pl = 0.2132$. For both cases $Bi = 2$, $K = 7$ and the emissivity of all the internal surfaces was set at $\epsilon = 0.6$. The mesh was composed by non-uniform hexaedrals, with a $h_{min} = 0.002$ located in the near-interface region and a $h_{max} = 0.04$ in the most distant zone to the walls of the domain. Two bodies were used: one for the heat source and the other for the conducting walls. For the radiative equation, the internal surfaces were divided in six, one for the bottom (heat source), one for the top, and the remaining four defined the lateral walls with $0.25 \times i < Z < 0.25 \times (i + 1)$ with $i = 0, 1, 2, 3$.

Temperature and vertical velocity distributions along the line $Y = Z = 0.5$ show good agreement with the reference case, as presented in Figure 4. Figure 5 show the streamlines, isotherms and a isovelocity contour plot for each case.

3.3. Case 3. Accuracy study

To the best of the authors' knowledge, there is no benchmark case available that includes a moving body, conjugate heat transfer and surface radiation. Therefore, a theoretical case with these characteristics was utilized to perform a numerical accuracy study. The test problem designed by Yang *et al.* [11] was adapted to include the thermal problem. The case consists of the two dimensional flow around a periodic array of cylinders moving with constant velocity V_C in a channel where the walls have a velocity of V_W (see Figure 6(a)). Since the cases with the same relative velocity $V_R = V_C - V_W$ are equivalent, the problem can be solved either with a static body or with a moving body. Hence, two combinations are considered: (i) static cylinder: $V_C = 0$ and $V_W = 1$, and (ii) moving cylinder: $V_C = -1$ and $V_W = 0$.

The diameter of the cylinder is D, the width of the channel is $L = 3 \times D$ and the separation between two cylinders is also L, as can be observed in Figure 6(a). The walls have constant temperature, $T_{left} = 0$ and $T_{right} = 1$ and the thermal conductivity ratio is $K = \lambda_{solid}/\lambda_{fluid} = 0.2$. The Reynolds number based on the diameter of the cylinder and the relative velocity $V_R = V_C - V_W$ is 100.

For the radiative equation, ten surfaces were defined: one is the right wall, another is the left wall and the remaining eight walls correspond to an equitative division of the cylinder. The emissivity of all the surfaces is set to $\epsilon = 0.7$ and the Planck number is $Pl = 0.05279$.

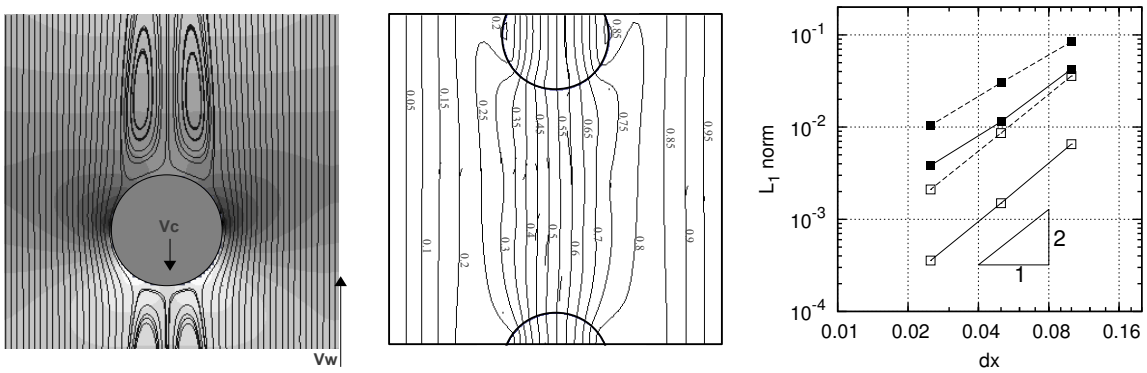

(a) (b) (c)

Figure 6. Flow around a periodic array of cylinders: (a) streamlines and pressure contour plot; (b) isothermal lines (c) norm of the error in velocity (□) and temperature (■) fields: continuous lines for static body and discontinuous lines for moving body.

A very fine mesh of 450×450 cells was used in order to compute the reference solution, with values of $V_C = 0$ and $V_W = 1$. Consequently, three other meshes of 30×30, 60×60 and 120×120 were employed to perform the accuracy study.

Pressure contour plots and streamlines are shown in Figure 6(a) and iso-temperature lines in Figure 6(b) for the moving cylinder case using a mesh of 60×60. The L_1 norm of the error, which measures the difference between the solutions from coarser grids and the reference grid is presented in Figure 6(c). The velocity and temperature fields respect the second order of the N-S solver as was expected. This is true for both configurations: moving and static cylinder, although the absolute error is larger for the moving cylinder case.

4. Conclusions and future work

An immersed-boundary method (IBM) for simulation of thermal flow problems including radiative surface exchange was presented. The validation of the code was performed through

the simulation of two cases from the literature. Moreover, an accuracy study was performed through a numerical experiment. A problem was designed so that it could be solved either with a moving immersed body or with a static immersed body. For both configurations the expected behavior of the method was observed, measuring a second order of accuracy for both velocity and temperature fields.

A monolithic-approach methodology has been proven to be successful in the solution of multiphysics problems, resulting especially appropriate for engineering applications, where the combination of various heat-transfer mechanisms is frequent. By representing the solid-fluid interfaces using unstructured surface meshes, the method can be applied for all kinds of geometries. Moreover, the domain mesh generation process is simplified, allowing to simulate several configurations with the same domain discretization.

Further work is needed to advance in the validation of more generic situations. A case including all the physics, with more complex geometry and with moving immersed bodies would be suitable. However, to the best of the authors' knowledge, there is not a benchmark case with these characteristics.

5. Acknowledgments

This work has been financially supported by the Ministerio de Economía y Competitvidad, Secretaría de Estado de Investigación, Desarrollo e Innovación, Spain (ENE-2014-60577-R), and by TermoFluids S.L. Additionally F. Favre wishes to thank the Agencia Nacional de Investigación e Innovación (ANII), Uruguay, for its financial support in the form of a doctoral degree scholarship.

References

[1] Lehmkuhl O, Perez-Segarra C, Borrell R, Soria M and Oliva A 2009 *Parallel Computational Fluid Dynamics 2007* 275–282
[2] Favre F, Antepara O, Lehmkuhl O, Borrell R and Oliva A 2014 *Proc. 11th World Congress on Computational Mechanics*
[3] Trias F and Lehmkuhl O 2011 *Numer. Heat Transfer* B **60** 116–34
[4] Fadlun E, Verzicco R, Orlandi P and Mohd-Yusof J 2000 *J. Comput. Phys.* **161** 35–60
[5] 3D Systems Inc. 1988 *Stereolithography Interface Specification* (3D Systems Inc., Valencia)
[6] Modest M F 2003 *Radiative Heat Transfer* (Academic Press)
[7] Miyanaga T and Nakano Y 2003 *Heat Transfer - Asian Research* **32** 108–29
[8] Saad Y and Schultz M H 1986 *SIAM J. Sci. and Stat. Comput.* **7** 856–69
[9] Hriberšek M and Kuhn G 2000 *Eng. Anal. Bound. Elem.* **24** 297–305
[10] Martyushev S G and Sheremet M A 2014 *Int. J. Heat Mass Transfer* **73** 340–53
[11] Yang J and Balaras E 2006 *J. Comput. Phys.* **215** 12–40